Enhanced electrochemical performance and durability for direct CH_4-CO_2 solid oxide fuel cells with an on-cell reforming layer

Peng Qiu[1], Xin Yang[2], Shichen Sun[2], Lichao Jia[3*], Jian Li[3] and Fanglin Chen[2*]

[1] School of Materials Science and Engineering, Shandong University of Science and Technology, Qingdao, 266590, China

[2] Department of Mechanical Engineering, University of South Carolina, Columbia, SC, 29208, United States

[3] Center for Fuel Cell Innovation, School of Materials Science and Engineering, State Key Lab of Material Processing and Die & Mound Technology, Huazhong University of Science and Technology, Wuhan, 430074, China

Abstract: Coking is a major issue with the traditional Ni-based anodes when directly oxidizing CH_4 in solid oxide fuel cells (SOFCs). Dry reforming to convert CH_4-CO_2 into CO-H_2 syngas before entering Ni-based anode may potentially be an effective and economical method to address the coking problem. Consequently, an on-cell reforming layer outside the Ni-based anode is expected to offer a unique solution for direct CH_4-CO_2 SOFCs without coking. In this study, Ni-GDC anode-supported cells with and without a $Sr_2Co_{0.4}Fe_{1.2}Mo_{0.4}O_{6-\delta}$ (SCFM) layer outside the anode support have been fabricated and evaluated using either H_2 or CH_4-CO_2 as fuel. Both types of cells show excellent electrochemical performance when H_2 is used as fuel, and the SCFM layer has negligible impact on the cell performance. When CH_4-CO_2 is used as fuel, however, the electrochemical performance and durability of the cells with the SCFM layer are much better than those without the SCFM layer outside the Ni-GDC anode, indicating that the SCFM layer can efficiently perform dry reforming. This unique on-cell dry reforming design enables direct CH_4-CO_2 solid oxide fuel cells and offers a very promising route for energy storage and conversion.

Keywords: coking, hydrocarbon fuel, on-cell reforming layer, electrochemical performance, durability

1. Introduction

As a new type of energy conversion device, solid oxide fuel cell (SOFC) has become a research focus recently because of its high electrical conversion efficiency, low emissions, and fuel flexibility[1-6]. In addition to the most commonly used hydrogen, hydrocarbon fuels such as ethanol and natural gas (with methane as the main component) can be directly used as the fuels in SOFCs. This significant advantage can greatly expand the fuel adaptability, reduce fuel cost and improve the safety of fuel storage, potentially accelerating the development and wide-spread adoption of SOFCs as distributed power stations and backup power sources. At present, the most commonly used SOFC anode materials are Ni-ceramic composites, which have the advantages of high catalytic activity for fuel oxidation, excellent electronic/thermal conductivity, good mechanical properties, and low price[7, 8]. In addition, when hydrocarbons are directly used as the fuel, Ni has a high catalytic activity for breaking C-H bonds. However, carbon deposition is a major issue for Ni-based anodes when directly oxidizing hydrocarbon fuels. Due to the high catalytic activity of Ni for forming carbon nanofibers or nanotubes[9-11], the surface of Ni particles is prone to be covered with carbon deposition, leading to gradual reduction in the catalytic activity of Ni and corresponding degradation of cell performance[12-14].

Extensive efforts have been devoted to solve the coking issue for Ni-based anodes, such as removing carbon by adding steam to hydrocarbon fuels[15-17], suppressing carbon deposition by adding precious metals or alloy particles to the anode[18-21], or adding materials with high ionic conductivity in the anode component. Alternatively, utilizing dry or wet reforming to convert hydrocarbon fuel into CO-H_2 syngas before hydrocarbon fuels entering the anode has been considered as a reliable, effective and economical method[22-24]. Moreover, an on-cell reforming layer outside the anode can further simplify the SOFC system and reduce the cost, thus greatly promoting the development of direct hydrocarbon SOFCs. Compared to the commonly adopted steam reforming, CO_2 dry reforming of hydrocarbon fuels has unique environmental and engineering benefits such as consuming greenhouse gases and preventing the fuel manifold from being corroded by steam. Although Ni-based anodes have been studied for dry reforming reaction, the reforming efficiency is insufficient[25, 26]. The low conversion rate of hydrocarbon will also inevitably lead to carbon deposition in the Ni-based anode even with the presence of CO_2 as the decoking agent.

As the main components of biogas, CH_4 and CO_2 can be easily obtained[27]. CO_2 dry reforming of CH_4 can convert the two major greenhouse gases into high-value CO-H_2 syngas. In addition, the heat generated from the electrochemical reactions as well as the ohmic heating from the solid oxide fuel cell operation can be directly utilized in the highly endothermic dry reforming reaction, thus achieving a thermally autogenous process[28-30]. Consequently, an on-cell reforming layer outside the anode is expected to be a promising design for direct CH_4-CO_2 SOFC without coking. In previous study, Ni-GDC anode-supported solid oxide fuel cells using GDC as the electrolyte and $La_{0.6}Sr_{0.4}Co_{0.2}Fe_{0.8}O_{3-\delta}$ (LSCF) as the cathode, with and without a highly catalytic active $La_{0.6}Sr_{0.2}Cr_{0.85}Ni_{0.15}O_3$ (LSCrN) on-cell reforming layer outside the Ni-GDC anode support have been studied. The excellent electrochemical performance and stability has been confirmed when fed with 50%CH_4-50%CO_2[31]. In this study, $Sr_2Co_{0.4}Fe_{1.2}Mo_{0.4}O_{6-\delta}$ (SCFM) was used as the on-cell reforming layer of LSCF//GDC//Ni+GDC single cells instead, and the influence of this reforming layer on cell performance was investigated when fed with H_2 or 50%CH_4-50%CO_2.

2. Experimental details

2.1 Material synthesis and single cell fabrication

SCFM powder for the on-cell reforming layer and LSCF powder for the cathode were synthesized by a sol-gel method, and the detailed synthesis procedures can be found in our previous study[32]. The chemical compatibility between SCFM and the anode was evaluated by heating up mixed powders of SCFM and NiO-GDC with a mass ratio of 1: 1 to 1100 °C in air for 24 h. The chemical stability of SCFM powder was evaluated by heat treatment at 700 °C in CO_2 for 24 h. The heat-treated products were then characterized using X-ray diffraction (XRD, Rigaku MiniFlex II) for crystalline phase analysis.

The anode-supported single cells have a cell configuration of Ni-GDC anode, GDC electrolyte and LSCF cathode. Half cells with anode support and electrolyte were prepared by die-pressing, dip-coating and co-sintering method. Briefly, commercial NiO (J. T. Baker), GDC (Fuel Cell Materials, U. S. A) and graphite with a mass ratio of 9:6:5 were ball-milled together for 12 h in ethanol medium. The obtained slurry was dried and then well-grounded with 3 wt% polyvinyl butyral (PVB, Butvar B-98, Sigma) as binder. Subsequently, the mixed powders were pressed into pellets using a stainless die. The obtained NiO-GDC pellets were pre-sintered at 900 °C for 2 h. The prepared

GDC electrolyte slurry was subsequently dip-coated onto one side of the pre-sintered NiO-GDC pellets. After drying, the pellets were sintered at 1450 °C for 6 h with the heating rate of 2 °C/min to obtain half cells with the configuration of NiO-GDC//GDC. Subsequently, LSCF cathode ink, with a mass ratio of LSCF: V006A (Heraeus, U. S. A) =1: 1, was painted onto the surface of the GDC electrolyte of the NiO-GDC//GDC half cells and calcined at 1050 °C for 2h. The obtained single cells with the configuration of LSCF//GDC//NiO-GDC were designated as conventional anode-supported cell (CASC). SCFM ink consisting of SCFM powder and V006A binder, with the mass ratio of 1: 1, was painted onto the surface of the anode support and calcined at 1050 °C for 2h. The obtained cell with the configuration of LSCF//GDC//NiO-GDC//SCFM was designated as double-layer anode supported cell (DASC).

2.2 Material characterizations

The phase compositions of the synthesized powders and chemical compatibility and stability tests were performed by XRD with Cu Kα radiation and a D/teX silicon strip detector. The step scan was operated from 20° to 80° in a step of 0.015° with the scanning rate of 6° min^{-1}. The microstructures of the single cells and SCFM on-cell reforming layer were characterized by field emission scanning electron microscopy (SEM, Zeiss Ultra Plus FESEM) equipped with energy-dispersive X-ray spectroscopy (EDS). The thermal expansion coefficient (TEC) of SCFM and NiO-GDC was measured using a thermal dilatometer (Netzsch DIL 420 PC/4). Raman spectrometry (Horiba Xplora Plus) was employed to detect deposited carbon in the anode support. To evaluate the catalytic performance of reduced SCFM or Ni-GDC, SCFM and NiO-GDC (with the mass ratio of 3:2) powders were placed in a quartz tube and reduced in H_2 at 850 °C for 5 h. Then the fed gas was switched to CH_4-CO_2 and the operation temperature was decreased to 700 °C. The exhaust gas was collected and analyzed by a gas chromatograph (GC, Agilent Technologies 490 Micro GC).

2.3 Single cell tests

Single cells were sealed onto an Al_2O_3 tube using ceramic paste (Ceramabond, Aremco Product, Inc.). Before sealing, Au paste was applied to the surface of the electrodes and then heat-treated at 600 °C for 1 h as the current collector. Before the electrochemical test, NiO-GDC support and SCFM layer were reduced *in situ* by 3%H_2O-H_2 at 850 °C for 5 h. Wet H_2 (3 mol%H_2O) or CH_4-CO_2 (1: 1) was supplied to

the anode at a flow rate of 20 ml min^{-1}, and the cathode was exposed to ambient air. Electrochemical impedance spectroscopy (EIS) and current density-voltage-powder density (I-V-P) curves were measured using an electrochemical test system (Versa STAT 3-400, Princeton Applied Research, U.S.A) at temperatures from 550 to 700 °C. In EIS measurements, the frequency range was from 10^6 Hz to 10^{-1} Hz and the signal amplitude was 10 mV, respectively. The durability tests of the single cells when fed with CH_4-CO_2 were conducted at 700 °C under the current density of 500 mA cm^{-2}.

3. Results and discussion

In our previous study, SCFM was used as the anode material of SOFC, and excellent coking resistance was achieved when CH_4 was used as the fuel[32]. Herein, SCFM is used as an on-cell reforming material, which is expected to improve the coking resistance of the anode-supported SOFC when CH_4-CO_2 is used as the fuel. SCFM presents a double perovskite structure in oxidizing atmophere[32]. In reducing atmosphere, however, SCFM will *in-situ* transform into a composite consisting of an alloy phase ($Co_{0.5}Fe_{0.5}$) and a Ruddlesden-Popper phase $Sr_3Co_{0.1}Fe_{1.3}Mo_{0.6}O_{7-\delta}$ (RP-SCFM), as shown in **Figure 1a**. This *in-situ* exsolution method to generate metal nanoparticles from perovskite oxide backbone has also been invesitigated in other studies[31, 33]. Previous study has shown that RP-SCFM can maintain excellent long-term stability in a reducing atmosphere[32]. **Figure 1b** shows the microstructure of SCFM skeleton in which a smooth surface is presented. Upon reduction, diversely and uniformly distributed nanoparticles appear on the surface of the parent oxide scalford, which can be seen in **Figure 1c**. Combined with the analysis of the EDS mapping images in **Figure 2** and XRD characterization, the exsolved nanoparticles are identified to be $Co_{0.5}Fe_{0.5}$ alloy.

As an on-cell catalytic reforming layer for anode-supported SOFC, SCFM should have matched TEC and excellent chemical compatibility with the anode support. The TEC values of SCFM and NiO-GDC between 600 and 1100 °C are 16.3×10^{-6} K^{-1} and 10.9×10^{-6} K^{-1}, respectively (**Figure 3a**). Despite the slight mismatch in TEC, the calcination temperature of 1050 °C is high enough to join the SCFM reforming layer with the NiO-GDC support. In addition, SCFM and GDC have excellent chemical compatibility below 1100 °C, as no chemical reaction was observed (**Figure 3b**).

Acceptable TEC matching and outstanding chemical compatibility ensure the reliability of the on-cell dry-reforming structure of anode-supported SOFC with a SCFM reforming layer. When heat-treated in CO_2 for 24 h at 700 °C, the phase composition of reduced SCFM has no change, showing excellent chemical stability of reduced SCFM against CO_2 (**Figure 3c**). When CH_4-CO_2 passed through the reduced SCFM layer at elevated temperatures, reduced SCFM will not react with CO_2. Although reduced SCFM contains Sr element that has a tendency to react with CO_2, the high-valence Mo at the B site is expected to stabilize the perovskite structure under CO_2-containing atmosphere[34, 35].

The catalytic performance of SCFM powder is shown in **Figure 4a** and **4b**. When CH_4-CO_2 passes through the reduced SCFM powder at 700 °C, most of CH_4 and CO_2 will be converted into H_2 and CO, presenting the high conversion rate of CH_4 and CO_2. Due to the excellent catalytic activity of reduced SCFM, CH_4 and CO_2 undergo a dry reforming reaction to form H_2 and CO (**Eq 1**), and the conversion rate of CH_4 and CO_2 can be as high as 90%, indicating the outstanding dry reforming efficiency of reduced SCFM. Moreover, the composition of the exhaust gas remains stable during the operation and the high conversion rate of CH_4 and CO_2 is well-maintained at ~90%, indicating the excellent catalytic stability of reduced SCFM. The excellent reforming efficiency can be attributed to the excellent catalytic activity of $Co_{0.5}Fe_{0.5}$ nanoparticles and abundant oxygen vacancies of the RP-SCFM phase. The strong interfacial interaction between the exsolved $Co_{0.5}Fe_{0.5}$ nanoparticles and the RP-SCFM substrate can suppress the formation of C-C bonds[36]. In addition, sufficient oxygen vacancies of the RP-SCFM oxide substrate are beneficial to the adsorption and dissociation of CO_2[36, 37], thus promoting the dry reforming reaction of CH_4-CO_2. The synergetic effects ensure the high catalytic durability for dry reforming of CH_4-CO_2. In contrast,

poor catalytic performance of Ni-GDC was observed compared to SCFM, as shown in **Figure 4c** and **4d**. Ni-GDC powder can catalyze both the dry reforming reaction of CH_4-CO_2 (**Eq 1**) and the C-H bond breaking of CH_4 (**Eq 2**). However, from the perspective of CO_2 conversion rate, the reforming efficiency is rather insufficient. As a catalyst, NiO-GDC is found to mainly catalyze the cracking of CH_4, which can be confirmed by the relatively high conversion rate of CH_4 compared to CO_2 (**Figure 4d)**. Moreover, at t=0 h, the CH_4 and CO_2 conversion rates are only 46.5% and 13%, respectively, which are much lower than that for the reduced SCFM. As operation time increases, CH_4 and CO_2 conversion rates become lower and lower. At t=18 h, the catalyst almost lost its catalytic activity, suggesting poor catalytic stability of the conventional NiO-GDC cermet for CH_4-CO_2 dry reforming.

$$CH_4 + CO_2 = 2H_2 + 2CO \quad (1)$$

$$CH_4 = C + 2H_2 \quad (2)$$

The cross-sectional microstructures of CASC are shown in **Figure 5a**, **5b** and **5c**. LSCF cathode has a thickness of ~25 μm, and the high porosity of the electrodes facilitates the gas transportation. GDC electrolyte has a thickness of ~10 μm, and its dense structure isolates the direct contact between fuel and air. Before the electrochemical performance test, anode support is *in situ* reduced in H_2 at 850 °C for 5 h. When H_2 is used as the fuel, excellent electrochemical performance of CASC is obtained, which can be seen in **Figure 5d** and **5e**. The open circuit voltage (OCV) is in the range from 0.906 to 0.811 V and decreases with increasing operation temperature. The relatively low OCV values are attributed to the mixed electronic and ionic conductivity of GDC electrolyte in reducing environment[38, 39]. As shown in **Table 1**, the polarization impedance (R_p) values of CASC are 0.302, 0.181, 0.122 and 0.076 Ω cm^2 at 550, 600, 650 and 700 °C, respectively, and the corresponding peak power

density (*PPD*) values are 0.191, 0.370, 0.633 and 0.801 W cm^{-2}, respectively.

The cell structure of DASC is similar to that of CASC, except that an additional SCFM catalytic layer is added outside the anode support. **Figure 6a** and **6b** show the microstructure of DASC after reduction. The SCFM reforming layer has a thickness of ~20 μm and is in close contact with the anode support. When H_2 is used as the fuel, the electrochemical performance of DASC is almost the same as that of CASC, which can be seen in **Figure 6c** and **6d**. The *PPD* values are 0.809, 0.630, 0.364 and 0.197 W cm^{-2} at the operation temperature of 700, 650, 600 and 550 °C, respectively. This additional catalytic layer does not show significant impact on the electrochemical performance of the cell, mainly due to the excellent conductivity of reduced SCFM in reducing environment as demonstrated in our previous study[32].

However, the importance of the reforming layer is highlighted when CH_4-CO_2 is used as the fuel. The electrochemical performance and durability of DASC are much better than those of CASC, which can be seen in **Figure 7** and **Table 1**. The R_p value of CASC is 0.256 Ω cm^2 at 700 °C, which is 2.3 times of that for DASC under the same operation condition. In the meantime, the corresponding *PPD* values are 0.403 and 0.715 W cm^{-2} for CASC and DASC, respectively. The difference in electrochemical performance can be attributed to low concentration of H_2 and CO for CASC when CH_4-CO_2 is used as the fuel. As mentioned above, Ni-GDC anode has insufficient reforming efficiency, leading to low conversion rate for CH_4 and CO_2. When fed with CH_4-CO_2 for DASC, fuel is converted into H_2 and CO at a high conversion rate under the catalysis of SCFM. While for CASC, when fed with CH_4-CO_2, CH_4-CO_2 has a low conversion rate when entering the Ni-GDC anode. In addition to CO and H_2, the anode atmosphere also includes CH_4, CO_2, etc. The difference in fuel composition in the anode chamber is the reason for the difference in OCV. In addition, the durability of DASC and CASC is

drastically different, as shown in **Figure 7c**. When operated at a current density of 500 mA cm^{-2}, negligible change in the output voltage of DASC was observed, indicating excellent fuel cell performance durability under dry reforming operation. On the contrary, CASC showed poor fuel cell performance durability when operated at the same condition, as the output voltage decreased continuously over time. To understand the reasons for the difference of fuel cell performance durability, Raman spectroscopy and SEM of the anodes were carried out, as shown in **Figure 8**. The presence of D- and G-band peaks in the Raman spectroscopy for amorphous and graphitic carbon[40-42], respectively, indicates that carbon has been formed in the Ni-GDC anode of CASC. This is further confirmed by the SEM and corresponding EDS (**Figure 8d**, **8e** and **8f**), revealing the presence of carbon nanofibers. In the anode of CASCs, CH_4 undergoes a thermal cracking reaction because of the excellent catalytic activity of Ni for CH_4 cracking. The thermally cracked CH_4 then leads to the formation of carbon nanofibers on the Ni surface, covering surfaces of the Ni particles and causing the gradual loss of catalytic activity of Ni. Although O^{2-} coming from the electrolyte and fuel cell reaction products (H_2O and CO_2) can consume part of the carbon nanofibers during operation, complete removal of carbon deposition cannot be achieved. In contrast, Raman and SEM results show that there are no carbon nanofibers present in the Ni-GDC anode as well as the SCFM reforming layer of DASCs. Due to the high dry reforming efficiency and CH_4-CO_2 conversion rate with the SCFM reforming layer, before entering the anode of DASCs, CH_4-CO_2 can be converted into CO-H_2 syngas under the catalytic action of the SCFM layer. Moreover, the small amount of carbon nanofibers produced from CH_4 cracking can be easily removed by O^{2-} from the electrolyte, or fuel cell reaction products, thus obtaining excellent cell performance durability of DASC when CH_4-CO_2 is used as the fuel.

4. Conclusions

In a reducing atmosphere, SCFM can be transformed into a composite of $Co_{0.5}Fe_{0.5}$ nanoparticles homogeneously distributed on the surface of RP-SCFM. Reduced SCFM presents an outstanding dry reforming efficiency and catalytic durability for CH_4-CO_2 dry reforming compared with Ni-GDC. Consequently, SCFM can be used as the on-cell reforming catalyst for Ni-GDC anode-supported SOFCs. When H_2 is used as fuel, the SCFM reforming layer shows negligible effect on the electrochemical performance because of the excellent conductivity of reduced SCFM. When CH_4-CO_2 is used as fuel, enhanced electrochemical performance and durability of DASCs have been observed compared to CASCs. DASC has a smaller R_p and higher *PPD* compared with CASC, which can be attributed to the high dry reforming efficiency toward CH_4-CO_2 dry reforming from the reduced SCFM on-cell reforming layer. Furthermore, when operated at a current density of 500 mA cm^{-2}, DASC shows stable output voltage over time, suggesting excellent durability; however, CASC has poor durability when operated at the same condition. The insufficient reforming efficiency of Ni-GDC results in severe coking of the CASC anode, thus leading to its rapid degradation. For DASC, during operation, CH_4-CO_2 can be continuously and steadily converted into H_2-CO syngas without coking, resulting in excellent durability of DASC. This on-cell reforming layer design can provide a new direction for the development of solid oxide fuel cells directly utilizing CH_4-CO_2 as fuel.

Acknowledges

The financial supports from the U.S. National Science Foundation (DMR-1832809), the National Key Research & Development Program of China (2018YFE0124700, 2017YFE0129300) and the National Natural Science Foundation of China (51872103, U1910209, U1601207) are gratefully acknowledged.

References

[1] Stambouli AB, Traversa E. Solid oxide fuel cells (SOFCs): a review of an environmentally clean and efficient source of energy. Renewable and Sustainable Energy Reviews. 2002;6:433-55.

[2] Choudhury A, Chandra H, Arora A. Application of solid oxide fuel cell technology for power generation—A review. Renewable and Sustainable Energy Reviews.

2013;20:430-42.

[3] Liu M, Lynch ME, Blinn K, Alamgir FM, Choi Y. Rational SOFC material design: new advances and tools. Materials Today. 2011;14:534-46.

[4] Yu F, Han T, Wang Z, Xie Y, Wu Y, Jin Y, et al. Recent progress in direct carbon solid oxide fuel cell: Advanced anode catalysts, diversified carbon fuels, and heat management. International Journal of Hydrogen Energy. 2021;46:4283-300.

[5] Qiu P, Yang X, Zhu T, Sun S, Jia L, Li J. Review on core-shell structured cathode for intermediate temperature solid oxide fuel cells. International Journal of Hydrogen Energy. 2020;45:23160-73.

[6] Inac S, Unverdi SO, Midilli A. Global warming, environmental and sustainability aspects of a geothermal energy based biodigester integrated SOFC system. International Journal of Hydrogen Energy. 2020;45:35039-52.

[7] Sarantaridis D, Atkinson A. Redox Cycling of Ni-Based Solid Oxide Fuel Cell Anodes: A Review. Fuel Cells. 2007;7:246-58.

[8] Yamaji K, Kishimoto H, Xiong Y, Horita T, Sakai N, Brito ME, et al. Feasibility of Ni-based cermet anode for direct HC SOFCs: Fueling ethane at a low S/C condition to Ni–ScSZ anode-supported cell. Journal of Power Sources. 2006;159:885-90.

[9] Chen D, Christensen KO, Ochoa-Fernández E, Yu Z, Tøtdal B, Latorre N, et al. Synthesis of carbon nanofibers: effects of Ni crystal size during methane decomposition. Journal of Catalysis. 2005;229:82-96.

[10] De Jong KP, Geus JW. Carbon Nanofibers: Catalytic Synthesis and Applications. Catalysis Reviews. 2000;42:481-510.

[11] Chen P, Zhang H-B, Lin G-D, Hong Q, Tsai K. Growth of carbon nanotubes by catalytic decomposition of CH_4 or CO on a Ni—MgO catalyst. Carbon. 1997;35:1495-501.

[12] Khan MS, Lee S-B, Song R-H, Lee J-W, Lim T-H, Park S-J. Fundamental mechanisms involved in the degradation of nickel–yttria stabilized zirconia (Ni–YSZ) anode during solid oxide fuel cells operation: a review. Ceramics International. 2016;42:35-48.

[13] Gür TM. Critical Review of Carbon Conversion in “Carbon Fuel Cells”. Chemical Reviews. 2013;113:6179-206.

[14] Boldrin P, Ruiz-Trejo E, Mermelstein J, Bermúdez Menéndez JM, Ramírez Reina Ts, Brandon NP. Strategies for Carbon and Sulfur Tolerant Solid Oxide Fuel Cell Materials, Incorporating Lessons from Heterogeneous Catalysis. Chemical Reviews. 2016;116:13633-84.

[15] Ahmed K, Foger K. Kinetics of internal steam reforming of methane on Ni/YSZ-based anodes for solid oxide fuel cells. Catalysis Today. 2000;63:479-87.

[16] Takeguchi T, Kani Y, Yano T, Kikuchi R, Eguchi K, Tsujimoto K, et al. Study on steam reforming of CH_4 and C_2 hydrocarbons and carbon deposition on Ni-YSZ cermets. Journal of Power Sources. 2002;112:588-95.

[17] Offer GJ, Mermelstein J, Brightman E, Brandon NP. Thermodynamics and Kinetics of the Interaction of Carbon and Sulfur with Solid Oxide Fuel Cell Anodes. Journal of the American Ceramic Society. 2009;92:763-80.

[18] Kim H, Lu C, Worrell W, Vohs J, Gorte R. Cu-Ni Cermet Anodes for Direct Oxidation of Methane in Solid-Oxide Fuel Cells. Journal of The Electrochemical Society. 2002;149:A247-A50.

[19] Hibino T, Hashimoto A, Yano M, Suzuki M, Sano M. Ru-catalyzed anode materials for direct hydrocarbon SOFCs. Electrochimica Acta. 2003;48:2531-7.

[20] Babaei A, Zhang L, Liu E. Performance and carbon deposition over Pd nanoparticle catalyst promoted Ni/GDC anode of SOFCs in methane, methanol and ethanol fuels. International Journal of Hydrogen Energy. 2012;37:15301-10.

[21] Choudhary V, Rane V, Rajput A. Beneficial effects of cobalt addition to Ni-catalysts for oxidative conversion of methane to syngas. Applied Catalysis A: General. 1997;162:235-8.

[22] Tang P, Zhu Q, Wu Z, Ma D. Methane activation: the past and future. Energy & Environmental Science. 2014;7:2580-91.

[23] Lin Y, Zhan Z, Barnett SA. Improving the stability of direct-methane solid oxide fuel cells using anode barrier layers. Journal of Power Sources. 2006;158:1313-6.

[24] Sengodan S, Lan R, Humphreys J, Du D, Xu W, Wang H, et al. Advances in reforming and partial oxidation of hydrocarbons for hydrogen production and fuel cell applications. Renewable and Sustainable Energy Reviews. 2018;82:761-80.

[25] Zhan Z, Barnett SA. An Octane-Fueled Solid Oxide Fuel Cell. Science. 2005;308:844-7.

[26] Hua B, Li M, Chi B, Jian L. Enhanced electrochemical performance and carbon deposition resistance of Ni–YSZ anode of solid oxide fuel cells by in situ formed Ni–MnO layer for CH_4 on-cell reforming. Journal of Materials Chemistry A. 2014;2:1150-8.

[27] Hernández B, Martín M. Optimal process operation for biogas reforming to methanol: effects of dry reforming and biogas composition. Industrial & Engineering Chemistry Research. 2016;55:6677-85.

[28] Lau C, Tsolakis A, Wyszynski M. Biogas upgrade to syn-gas (H_2–CO) via dry and oxidative reforming. International Journal of Hydrogen Energy. 2011;36:397-404.

[29] Hua B, Yan N, Li M, Zhang Y-q, Sun Y-f, Li J, et al. Novel layered solid oxide fuel cells with multiple-twinned $Ni_{0.8}Co_{0.2}$ nanoparticles: the key to thermally independent CO_2 utilization and power-chemical cogeneration. Energy & Environmental Science. 2016;9:207-15.

[30] Li M, Hua B, Luo J-L. Alternative Fuel Cell Technologies for Cogenerating Electrical Power and Syngas from Greenhouse Gases. ACS Energy Letters. 2017;2:1789-96.

[31] Wei T, Qiu P, Yang J, Jia L, Chi B, Pu J, et al. High-performance direct carbon dioxide-methane solid oxide fuel cell with a structure-engineered double-layer anode. Journal of Power Sources. 2021;484:229199.

[32] Qiu P, Yang X, Wang W, Wei T, Lu Y, Lin J, et al. Redox-Reversible Electrode Material for Direct Hydrocarbon Solid Oxide Fuel Cells. ACS Applied Materials & Interfaces. 2020;12:13988-95.

[33] Liu Y, Jia L, Li J, Chi B, Pu J, Li J. High-performance Ni in-situ exsolved $Ba(Ce_{0.9}Y_{0.1})_{0.8}Ni_{0.2}O_{3-\delta}/Gd_{0.1}Ce_{0.9}O_{1.95}$ composite anode for SOFC with long-term

stability in methane fuel. Composites Part B: Engineering. 2020;193:108033.

[34] Fernández-Ropero A, Porras-Vázquez J, Cabeza A, Slater P, Marrero-López D, Losilla E. High valence transition metal doped strontium ferrites for electrode materials in symmetrical SOFCs. Journal of Power Sources. 2014;249:405-13.

[35] Xie K, Zhou J, Meng G. Pervoskite-type $BaCo_{0.7}Fe_{0.2}Ta_{0.1}O_{3-\delta}$ cathode for proton conducting IT-SOFC. Journal of Alloys and Compounds. 2010;506:L8-L11.

[36] Wei T, Jia L, Luo J, Chi B, Pu J, Li J. CO_2 dry reforming of CH_4 with Sr and Ni co-doped $LaCrO_3$ perovskite catalysts. Applied Surface Science. 2019;506:144699.

[37] Solymosi F. The bonding, structure and reactions of CO_2 adsorbed on clean and promoted metal surfaces. Journal of Molecular Catalysis. 1991;65:337-58.

[38] Mogensen M, Sammes NM, Tompsett GA. Physical, chemical and electrochemical properties of pure and doped ceria. Solid State Ionics. 2000;129:63-94.

[39] Park S-H, Yoo H-I. Thermoelectric behavior of a mixed ionic electronic conductor, $Ce_{1-x}Gd_xO_{2-x/2-\delta}$. Physical Chemistry Chemical Physics. 2009;11:391-401.

[40] Cuesta A, Dhamelincourt P, Laureyns J, Martinez-Alonso A, Tascón JD. Raman microprobe studies on carbon materials. Carbon. 1994;32:1523-32.

[41] Watanabe S, Shinohara M, Kodama H, Tanaka T, Yoshida M, Takagi T. Amorphous carbon layer deposition on plastic film by PSII. Thin Solid Films. 2002;420:253-8.

[42] Hua B, Li M, Pu J, Chi B, Jian L. $BaZr_{0.1}Ce_{0.7}Y_{0.1}Yb_{0.1}O_{3-\delta}$ enhanced coking-free on-cell reforming for direct-methane solid oxide fuel cells. Journal of Materials Chemistry A. 2014;2:12576-82.

Figure Captions

Figure 1 (a) XRD patterns of as-prepared SCFM and reduced SCFM powder; (b) Microstructure of SCFM skeleton; (c) Microstructure of reduced SCFM skeleton.

Figure 2 EDS mapping images of reduced SCFM powder.

Figure 3 (a) TEC of SCFM and NiO-GDC; (b) Chemical compatibility between SCFM and GDC at 1100 °C; (c) Chemical compatibility between reduced SCFM and CO_2 at 700 °C.

Figure 4 (a, b) The composition of exhaust gas from reduced SCFM and corresponding CH_4/CO_2 conversion rate at different operation time; (c, d) The composition of exhaust gas from Ni-GDC and corresponding CH_4/CO_2 conversion rate at different operation time.

Figure 5 (a) Microstructure of CASC single cell; (b) Microstructure of LSCF cathode; (c) Microstructure of Ni-GDC anode support after reduction; (d) EIS of CASC single cell at the operation temperature of 550, 600, 650 and 700 °C when fed with H_2; (e) I-V-P curves of CASC single cell at the operation temperature of 550, 600, 650 and 700 °C when fed with H_2.

Figure 6 (a) Microstructure of DASC single cell; (b) Microstructure of SCFM-anode support interface; (c) EIS of DASC single cell at the operation temperature of 550, 600, 650 and 700 °C when H_2 is used as the fuel; (d) I-V-P curves of DASC single cell at the operation temperature of 550, 600, 650 and 700 °C when fed with H_2.

Figure 7 The electrochemical behavior of DASC and CASC at 700 °C when fed with CH_4-CO_2: (a) EIS; (b) I-V-P curves; (c) Durability tests at the current density of 500 mA cm^{-2}.

Figure 8 Characterization and analysis of Ni-GDC anode supports of CASC and DASC after durability tests: (a) Raman spectra; (b) Microstructure of anode supports of DASC; (c) Microstructure of SCFM reforming layer of DASC; (d, e) Microstructure of anode supports of CASC; and (f) EDS of blue area in (e).

Table 1 The performance of CASC and DASC at different operating temperature when fed with H_2 or CH_4-CO_2.

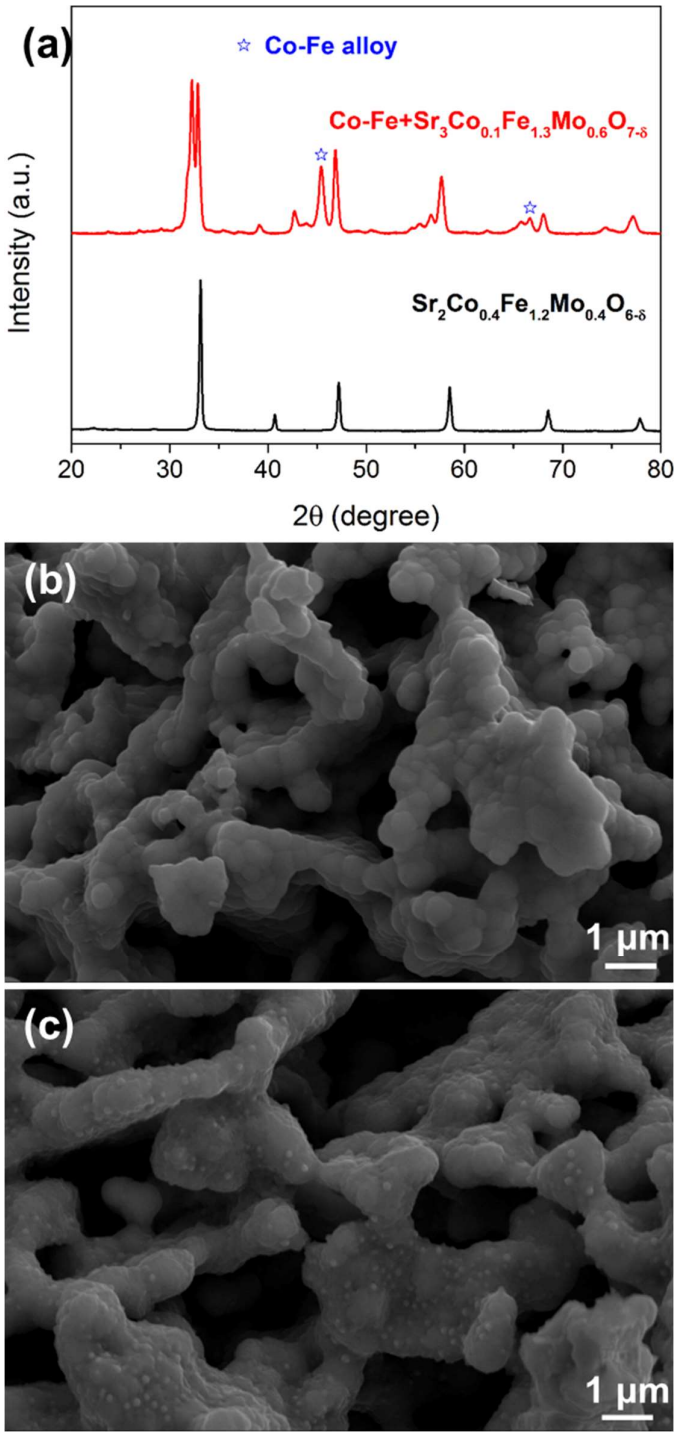

Figure 1 (a) XRD patterns of as-prepared SCFM and reduced SCFM powder; (b) Microstructure of SCFM skeleton; (c) Microstructure of reduced SCFM skeleton.

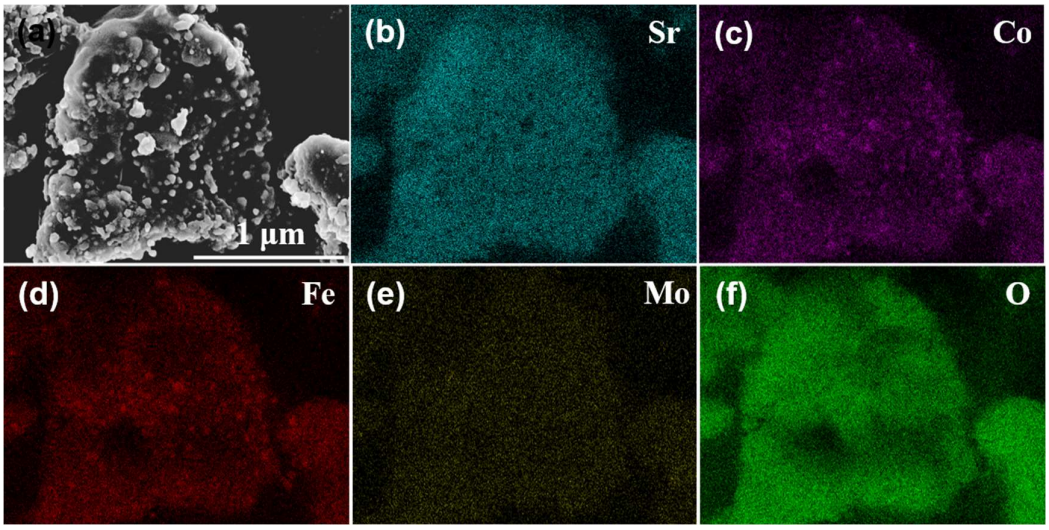

Figure 2 EDS mapping images of reduced SCFM powder.

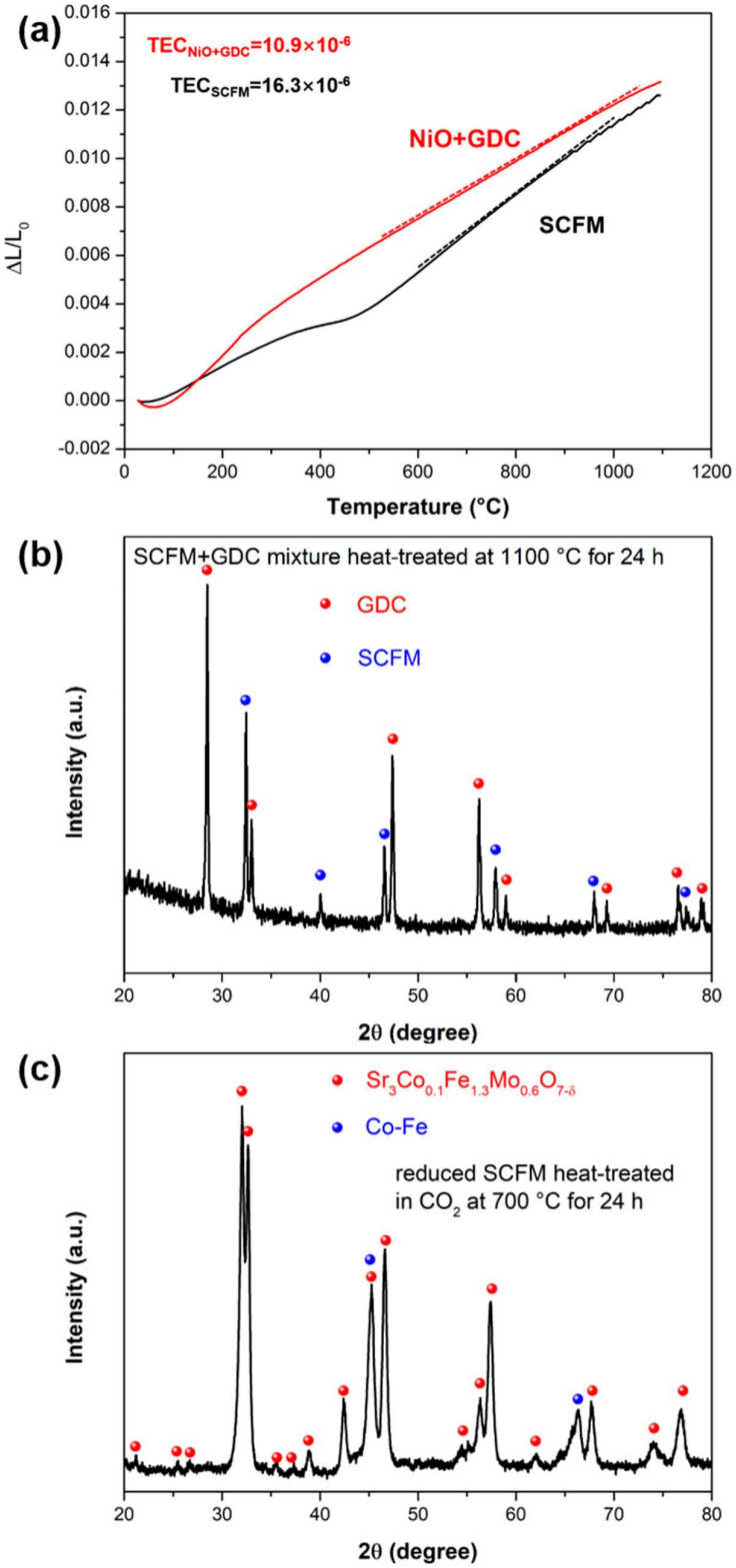

Figure 3 (a) TEC of SCFM and NiO-GDC; (b) Chemical compatibility between SCFM and GDC at 1100 °C; (c) Chemical compatibility between reduced SCFM and CO_2 at 700 °C.

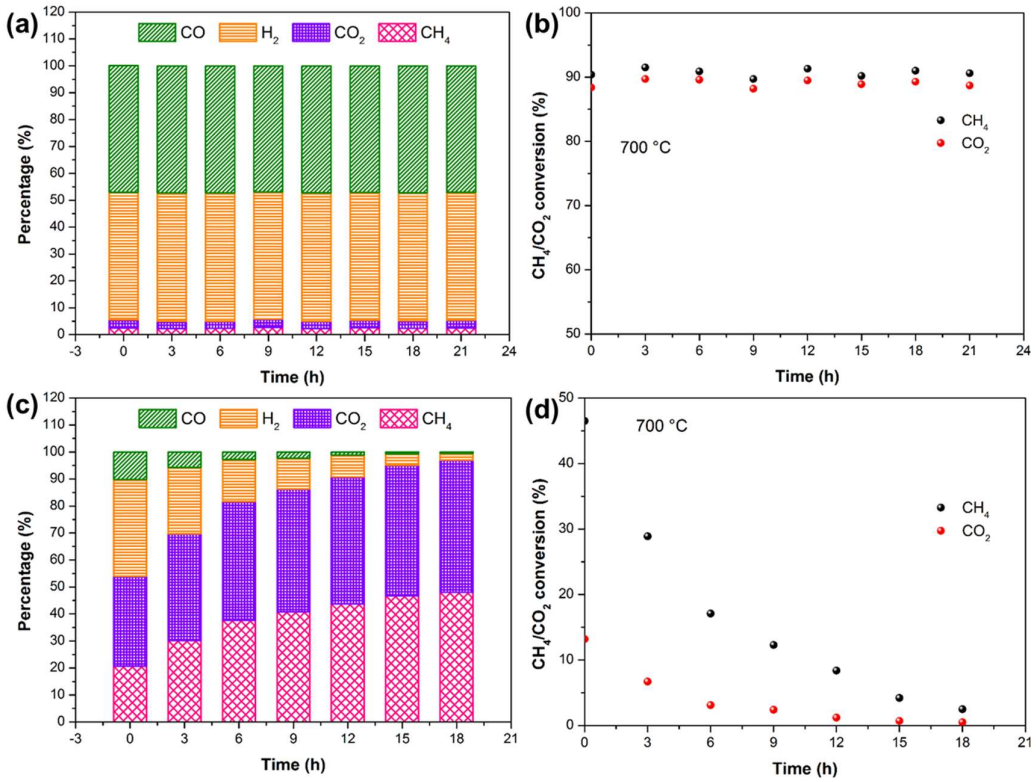

Figure 4 (a, b) The composition of exhaust gas from reduced SCFM and corresponding CH_4/CO_2 conversion rate at different operation time; (c, d) The composition of exhaust gas from Ni-GDC and corresponding CH_4/CO_2 conversion rate at different operation time.

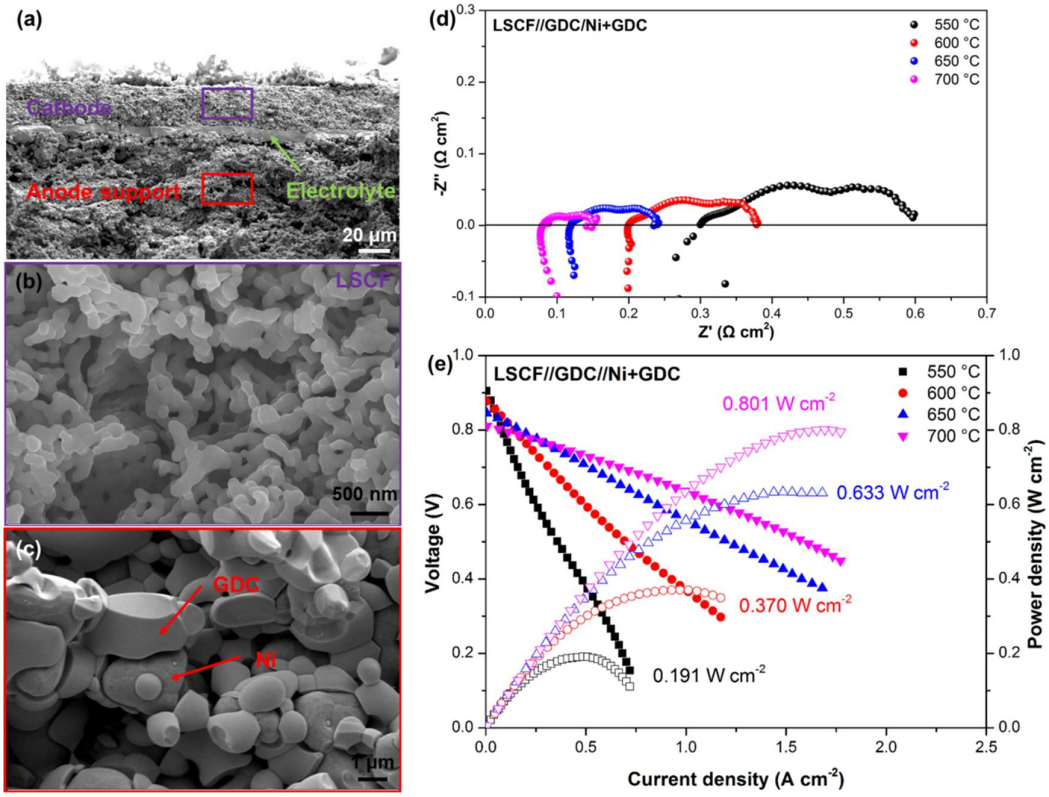

Figure 5 (a) Microstructure of CASC single cell; (b) Microstructure of LSCF cathode; (c) Microstructure of Ni-GDC anode support after reduction; (d) EIS of CASC single cell at the operation temperature of 550, 600, 650 and 700 °C when fed with H_2; (e) I-V-P curves of CASC single cell at the operation temperature of 550, 600, 650 and 700 °C when fed with H_2.

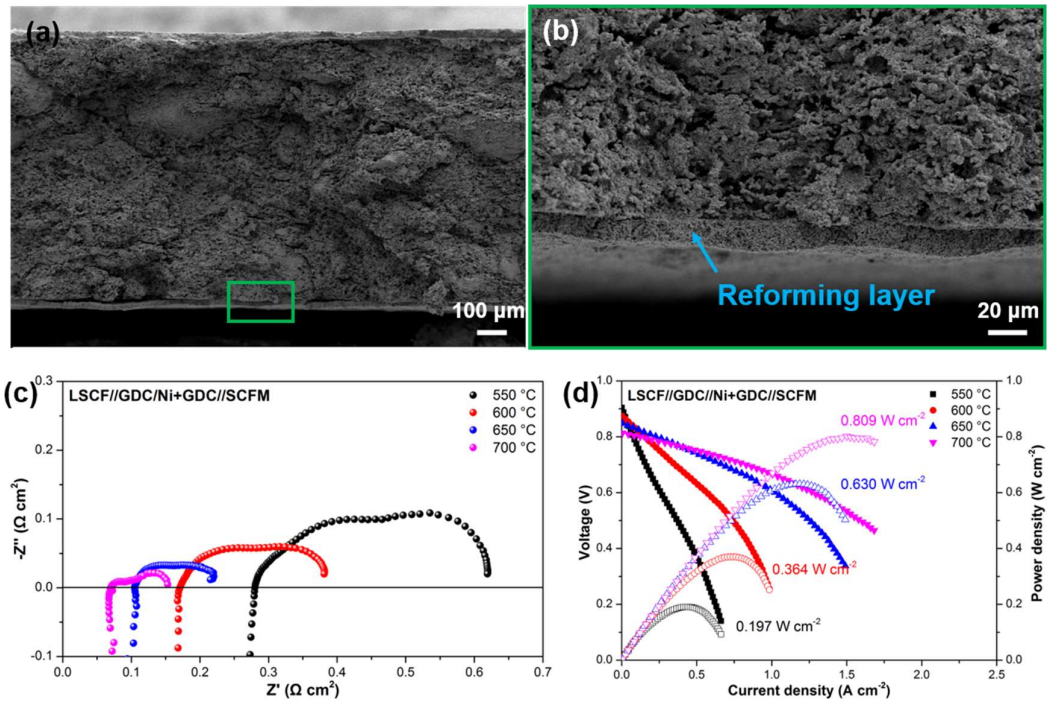

Figure 6 (a) Microstructure of DASC single cell; (b) Microstructure of SCFM-anode support interface; (c) EIS of DASC single cell at the operation temperature of 550, 600, 650 and 700 °C when H_2 is used as the fuel; (d) I-V-P curves of DASC single cell at the operation temperature of 550, 600, 650 and 700 °C when fed with H_2.

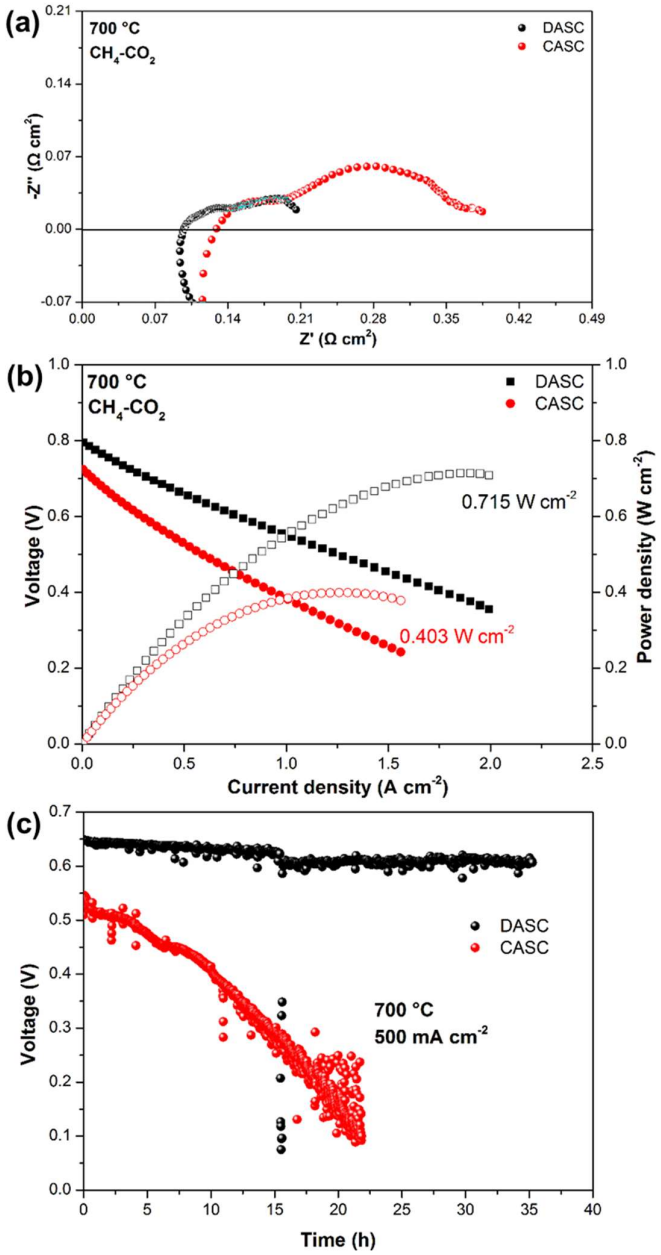

Figure 7 The electrochemical behavior of DASC and CASC at 700 °C when fed with CH_4-CO_2: (a) EIS; (b) I-V-P curves; (c) Durability tests at the current density of 500 mA cm^{-2}.

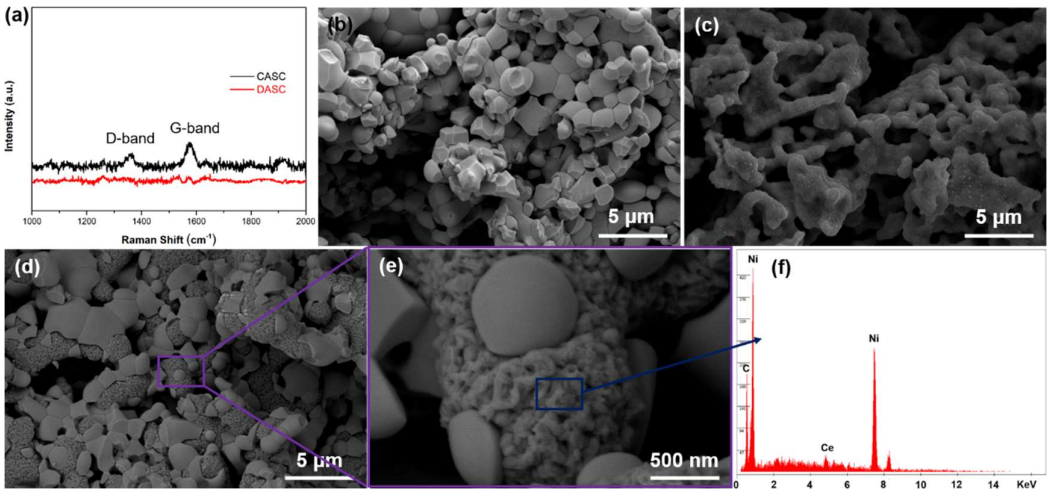

Figure 8 Characterization and analysis of Ni-GDC anode supports of CASC and DASC after durability tests: (a) Raman spectra; (b) Microstructure of anode supports of DASC; (c) Microstructure of SCFM reforming layer of DASC; (d, e) Microstructure of anode supports of CASC; and (f) EDS of blue area in (e).

Table 1 The performance of CASC and DASC at different operating temperature when fed with H_2 or CH_4-CO_2.

		H_2		CH_4-CO_2	
		CASC	DASC	CASC	DASC
550	R_p	0.297	0.3391	-	-
	PPD	0.191	0.197	-	-
600	R_p	0.178	0.21	-	-
	PPD	0.370	0.364	-	-
650	R_p	0.117	0.115	-	-
	PPD	0.633	0.630	-	-
700	R_p	0.068	0.083	0.255	0.108
	PPD	0.801	0.809	0.403	0.715